Int. J. Solids Structures, 1969, Vol. 5, pp. 713 to 725. Pergamon Press. Printed in Great Britain

THE EFFECT OF YIELD SURFACES ON THE LIMIT PRESSURE OF INTERSECTING SHELLS

FERNAND ELLYIN

Département de génie civil, Université de Sherbrooke, Sherbrooke, Quebec, Canada

Abstract—A complete solution is obtained for a rigid-plastic, cylinder–sphere intersecting shell subjected to internal pressure. The solution is presented in such a way that it enables one to compare the limit pressure, calculated on the basis of the uniform Tresca yield surface which is nonlinear, with the other linearized surfaces. It is shown that the limited-interaction yield surface, which has been used frequently, is not a good approximation for small diameter ratios, D/d and/or thin shell where T/D is small. Some experimental evidence is also presented in support of these conclusions.

1. INTRODUCTION

SOLUTIONS based on limit analysis of the title problem have been given by Lind [1], Gill [2], Ellyin and Sherbourne [3] and others. The salient differences among these solutions and their shortcomings are detailed in Refs. [4, 5]. With the exception of Ref. [1], hexagonal yield surface (often termed "one-moment limited-interaction") proposed by Drucker and Shield [6] has been employed. Contrary to elastic solutions (see Ref. [7] for a summary of them), the limit analysis approach is quite simple, and can provide a basis for rational design of intersecting shell problems. These problems are of special interest to pressure vessel, piping, and nuclear reactor industries.

The purpose of this paper is, (a) to present a complete solution for the cylinder–sphere intersecting shell with uniform Tresca yield surface, (b) to formulate the problem in such a way that it would enable one to use various yield surfaces and compare the results, and (c) to establish the range of applicability of piecewise linear and approximate yield surfaces, in terms of shell parameters.

2. STATEMENT AND FORMULATION OF THE PROBLEM

Consider a surface of revolution obtained by the intersection of a circular cylinder and a spherical shell, Fig. 1, which is termed hereafter as an "intersecting shell". The shell material is assumed to be rigid–perfectly-plastic, obeying Tresca's (maximum shearing stress) yield criterion and associated flow rule. The state of stress at a generic point of the intersecting shell is assumed to be two-dimensional and due to rotational symmetry, circumferential and meridional planes are principal planes of stress. Tresca's yield condition and the associated flow rule are summarized in Fig. 2, where subscripts θ and (φ or x) refer to circumferential and meridional directions, respectively.

Let the intersecting shell be subjected to the normal pressure P, which is slowly increased from zero. For sufficiently small values of P, stresses everywhere will be below the yield stress σ_0, so that the strains are zero. In this stage, the stress distribution cannot be uniquely

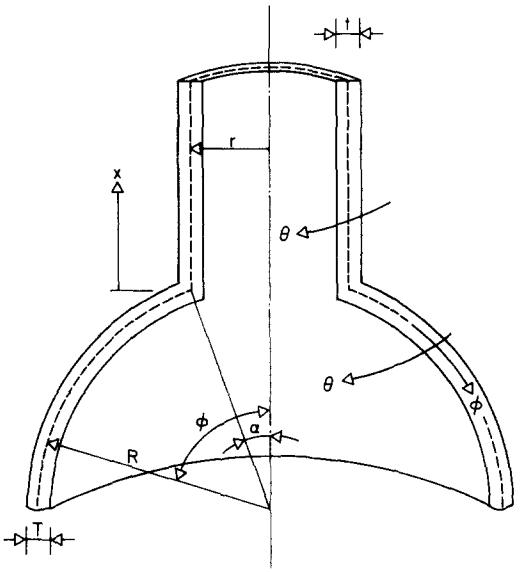

FIG. 1. Typical cross section of an intersecting shell with directional and dimensional notation.

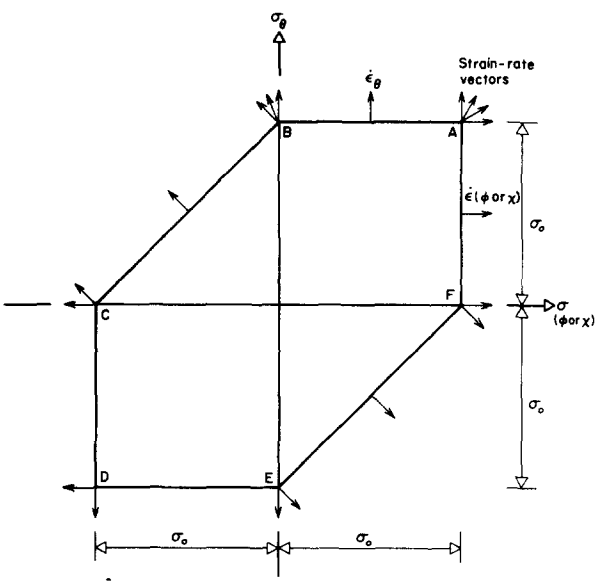

FIG. 2. Tresca yield condition and flow rule for plane stress.

determined. When the pressure reaches a certain value, the intersecting shell will begin to deform near the junction (localized region of high stress concentration). In this region the circumferential stress σ_θ reaches σ_0 and a small increment of pressure will result in an almost constant circumferential stress distribution throughout the wall thickness. The meridional stress $\sigma_{(\varphi \text{ or } x)}$ at the outer surface and part of wall thickness will also reach σ_0 in junction. The plastic region, however, will be forced to remain rigid as a result of constraints exerted from

the surrounding rigid portions of the intersecting shell, whereas if left to itself, it could flow plastically. It is convenient to speak of a "hinge circle" forming in this region.

As P is further increased, the plastic region near the junction will start to grow. However, the deformations will continue to be small until there is sufficient amount of plasticity spread in both directions so that the surrounding rigid portions are unable to restrain plastic region from motion. This situation may be described by yielding taking place in meridional plane at two additional locations. This will constitute a "mechanism" which will permit motion of part of the intersecting shell. Collapse occurs only when the formation of the mechanism is complete. The problem therefore, is to determine the limit pressure P_0 or bounds of it.

Lower bound analysis

The equations of equilibrium with the notation of Fig. 3, for the cylindrical part are given by:

$$\frac{dQ_x}{dx} = P - \frac{N_\theta}{r} \tag{1a}$$

$$\frac{dM_x}{dx} = Q_x \tag{1b}$$

$$\frac{dN_x}{dx} = 0 \tag{1c}$$

whereas for the spherical part we have,

$$N_\varphi \sin\varphi + Q_\varphi \cos\varphi = \tfrac{1}{2}PR\sin\varphi \tag{2a}$$

$$N_\varphi \sin\varphi + N_\theta \sin\varphi + \frac{d}{d\varphi}(Q_\varphi \sin\varphi) = PR\sin\varphi \tag{2b}$$

$$\frac{dM_\varphi}{d\varphi}\sin\varphi + (M_\varphi - M_\theta)\cos\varphi - Q_\varphi R\sin\varphi = 0 \tag{2c}$$

Any system of moments and membrane forces which satisfies the above equilibrium equations and the stress boundary conditions and does not violate yield condition, will provide a lower bound on the limit load.

The foregoing discussion of the behavior of the intersecting shell under slowly increasing pressure suggests that at the limit load or just before it is reached, σ_θ is equal to σ_0 throughout the thickness. This implies that the stress profile lies on the face of the yield surface represented by the segment AB of Fig. 2. In the analysis to follow, body forces, dynamic actions, thermal effects and the variation of the pressure are neglected.

Equations (1) now can be integrated by taking $N_\theta = \sigma_0 t$, which leads to,

$$N_x = \tfrac{1}{2}Pr \tag{3a}$$

$$Q_x = \left(P - \frac{\sigma_0 t}{r}\right)x + A_1 \tag{3b}$$

$$M_x = \frac{1}{2}\left(P - \frac{\sigma_0 t}{r}\right)x^2 + A_1 x + A_2 \tag{3c}$$

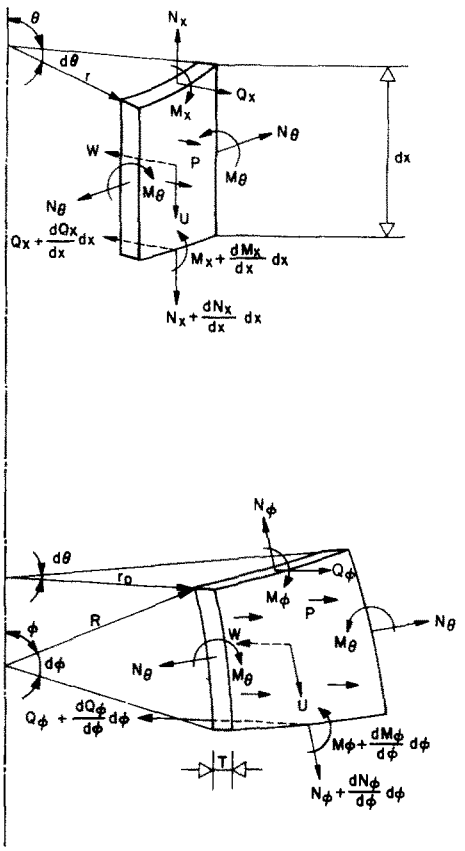

FIG. 3. Elements of cylindrical and spherical shells with notation and positive direction of forces acting on them.

where A_1 and A_2 are constants of integration. Similarly, for the spherical part $N_\theta = \sigma_0 T$* and this will require that M_θ be equal to zero. Hence the integration of equation (2) leads to

$$N_\varphi = \frac{1}{2}PR + \left[\frac{R}{2}\left(\frac{2\sigma_0 T}{R} - P\right)\varphi - B_1\right]\cot\varphi \tag{4a}$$

$$Q_\varphi = -\frac{R}{2}\left(\frac{2\sigma_0 T}{R} - P\right)\varphi + B_1 \tag{4b}$$

$$M_\varphi = R\left[\frac{R}{2}\left(\frac{2\sigma_0 T}{R} - P\right)(\varphi\cot\varphi - 1)\right] - B_1 R\cot\varphi + B_2\operatorname{cosec}\varphi \tag{4c}$$

where B_1 and B_2 are constants of integration.

The equilibrium of shear and membrane forces at the junction results in the following identity:

$$P = \frac{2}{r}(Q_0\sin\alpha + Q_\alpha)\sec\alpha \tag{5}$$

* It is not necessary that the yield stress σ_0 of the both cylindrical and spherical parts be equal. One may assume that the yield stress for the spherical part is $\sigma_0^s = \gamma\sigma_0^c$ where σ_0^c is the yield stress of the cylindrical part and $\gamma \geq 1$ or ≤ 1. However for very small or great values of γ, the mechanism will not be the one assumed here and it may be confined to one part only.

where Q_0 and Q_α are the shear forces in cylindrical and spherical parts at the junction respectively. These forces have to be evaluated from equations (3) and (4). For the determination of four constants of integration A_1, A_2, B_1 and B_2, the following stress boundary conditions are assumed:

For the cylindrical part,

$$\begin{aligned} &\text{at} \quad x = 0, \qquad Q_x = Q_0, \qquad M_x = M_k, \\ &\text{at} \quad x = l, \qquad Q_x = 0, \qquad M_x = M_c. \end{aligned} \tag{6}$$

For the spherical part,

$$\begin{aligned} &\text{at} \quad \varphi = \alpha, \qquad Q_\varphi = Q_\alpha, \qquad M_\varphi = M_k, \\ &\text{at} \quad \varphi = \beta, \qquad Q_\varphi = \frac{M_s}{R}\cot\beta, \qquad M_\varphi = M_s \end{aligned} \tag{7}$$

where M_k, M_c and M_s are appropriate meridional moments on the yield surface. l and β, may designate the location of external boundaries, which in this instance are considered as locations of the hinge circles in the cylindrical and spherical parts respectively. It can easily be seen, by differentiating equations (3c) and (4c) that at $x = l$ and $\varphi = \beta$, the meridional bending moments are maximum at the cylindrical and spherical parts respectively.*

Evaluating constants of integration with the help of boundary conditions (6) and (7) and then substituting for Q_0 and Q_α in equation (5) yields:

$$P = (2/r)\left\{\left[2(M_c - M_k)\left(\frac{\sigma_0 t}{r} - P\right)\right]^{\frac{1}{2}} \sin\alpha + \frac{R}{2}\left(\frac{2\sigma_0 T}{R} - P\right)(\beta - \alpha) + \frac{M_s}{R}\cot\beta\right\}\sec\alpha, \tag{8a}$$

where

$$\beta = \alpha - \left[1 + \frac{2}{R^2}\left(\frac{2\sigma_0 T}{R} - P\right)^{-1} M_k\right]\tan\alpha + \left[1 + \frac{2}{R^2}\left(\frac{2\sigma_0 T}{R} - P\right)^{-1} M_s\right]\sin\beta\sec\alpha$$
$$- \frac{2M_s}{R^2}(1 - \cos\beta\sec\alpha)\left(\frac{2\sigma_0 T}{R} - P\right)^{-1}\cot\beta, \tag{8b}$$

$$l = \left[2(M_c - M_k)\left(\frac{\sigma_0 t}{r} - P\right)^{-1}\right]^{\frac{1}{2}} \tag{8c}$$

It may be noted that equations (8) contain meridional moments M_c, M_k and M_s and until the present nothing has been indicated regarding their values. The values of the meridional moments are not entirely arbitrary, and for the assumed yield condition and the stress distribution of fully plastic section due to σ_θ, a stress distribution of an element is shown in Fig. 4. The resulting plane section of the yield surface is therefore defined by

$$N_\theta = N_0, \qquad M_\theta = 0, \qquad -2\frac{N_{(\varphi \text{ or } x)}}{N_0}\left(1 - \frac{N_{(\varphi \text{ or } x)}}{N_0}\right) \leq \frac{M_{(\varphi \text{ or } x)}}{M_0} \leq 2\frac{N_{(\varphi \text{ or } x)}}{N_0}\left(1 - \frac{N_{(\varphi \text{ or } x)}}{N_0}\right) \tag{9}$$

* The shearing force Q_x equals zero at the hinge location in the cylindrical part and this is evident from equation (1b). It is not possible to draw a similar conclusion for the shearing force Q_φ at the hinge location in the spherical part, as it can be seen from equation (2c). Thus Dinno and Gill's analysis [8] is incorrect as far as the boundary conditions for the spherical part are concerned.

where N_0 and M_0 are the maximum plastic moment and membrane force respectively for each part of the intersecting shell.

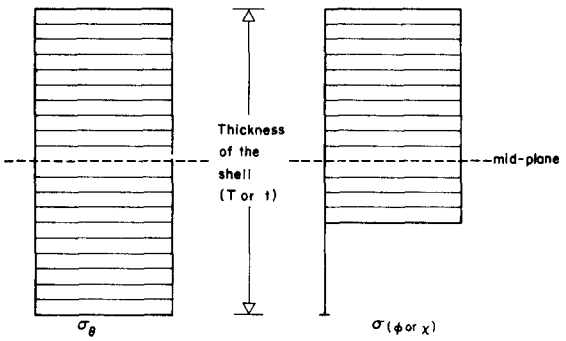

FIG. 4. Stress distribution in critical sections at limit pressure.

In the light of the above yield condition, the appropriate values of the meridional bending moments appearing in the equations (8) are given by:

$$M_c = \frac{1}{4}Prt\left(1-\frac{Pr}{2\sigma_0 t}\right) \tag{10a}$$

$$M_s = b+\left[b^2+\tfrac{1}{4}P^2R^4\left(2\frac{\sigma_0 T}{PR}-1\right)\tan^4\beta\right]^{\frac{1}{2}} \tag{10b}$$

$$M_k = -\min(M_c, M_s) \tag{10c}$$

where

$$b = \frac{1}{2}PR^2\tan^2\beta\left(1-\frac{\sigma_0 T}{PR}-2\frac{\sigma_0}{P}\tan^2\beta\right)$$

However, if Hodge's two-moment limited-interaction surface [9] is chosen to represent the yield condition in the generalized stress space, then the values of meridional bending moments in equations (8) are given by:

$$M_c = \tfrac{1}{4}\sigma_0 t^2, \qquad M_s = \tfrac{1}{4}\sigma_0 T^2, \qquad M_k = -\tfrac{1}{4}\sigma_0 \min(t^2, T^2). \tag{11}$$

Similarly for any other yield surface, the moments can easily be calculated. Of course, the condition on the stress profile to lie on the specific portion of yield surface will impose certain restrictions on the shell geometry, which will be discussed later.

Figure 5 shows the collapse mechanism consisting of three hinge circles. For the cylindrical part of the shell, the velocity field is given by:

$$u = \begin{cases} u_0 \\ 0 \end{cases} \qquad w = \begin{cases} -w_0(1-x/l) & \text{for} \quad x < l \\ 0 & \text{for} \quad x \geq l. \end{cases} \tag{12}$$

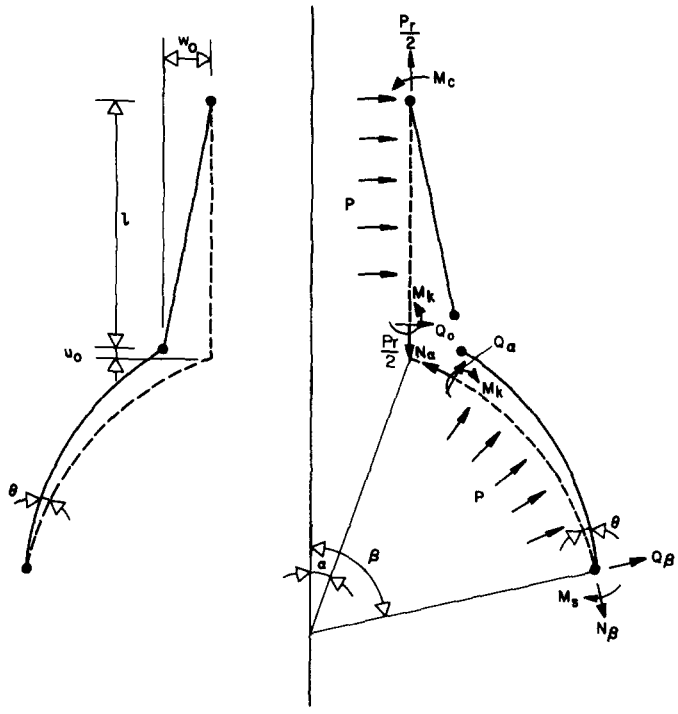

FIG. 5. The collapse mechanism consisting of three hinge circles.

Insertion of these velocities in the strain-rate–velocity relations, leads to:
for $x < l$

$$\dot{\varepsilon}_x = \frac{du}{dx} = 0, \qquad \dot{\chi}_x = -\frac{\partial^2 w}{\partial x^2} = 0,$$
$$\dot{\varepsilon}_\theta = -\frac{w}{r} = \frac{w_0}{rl}(l-x), \qquad \dot{\chi}_\theta = 0. \tag{13}$$

whereas for $x \geq l$ all the strain-rates are obviously zero.

Similarly, for the spherical part, the associated velocities are:

$$u = \begin{cases} \theta R[1-\cos(\beta-\varphi)] \\ 0 \end{cases} \qquad w = \begin{cases} -\theta R \sin(\beta-\varphi) & \text{for } \varphi < \beta \\ 0 & \varphi \geq \beta \end{cases} \tag{14}$$

for which the corresponding strain-rates become

$$\dot{\varepsilon}_\varphi = \frac{1}{R}\left(\frac{du}{d\varphi} - w\right) = 0, \qquad \dot{\chi}_\varphi = \frac{1}{R^2}\frac{d}{d\varphi}\left(u + \frac{dw}{d\varphi}\right) = 0$$
$$\dot{\varepsilon}_\theta = \frac{1}{R}(u\cot\varphi - w) = \frac{\theta}{\sin\varphi}(\cos\varphi - \cos\beta), \qquad \dot{\chi}_\theta = \frac{\cot\varphi}{R^2}\left(u + \frac{dw}{d\varphi}\right) = \frac{\theta}{R}\cot\varphi \tag{15}$$

here too, the strain-rates are zero for region $\varphi \geq \beta$.

Assuming the Kirchhoff hypothesis, we may express the distribution of principal strain rates of the shell in the form

$$\dot{e}_\theta = \dot{\varepsilon}_\theta + \dot{\chi}_\theta z, \qquad \dot{e}_{(\varphi \text{ or } x)} = \dot{\varepsilon}_{(\varphi \text{ or } x)} + \dot{\chi}_{(\varphi \text{ or } x)} z. \tag{16}$$

Substituting from (13) in (16), the strain-rate distribution for the cylindrical part is.

$$\dot{e}_\theta = \frac{w_0}{lr}(l-x), \qquad \dot{e}_x = 0. \tag{17}$$

by which the corresponding state of stress is represented by segment AB of Fig. 2, throughout the thickness for the region bounded by $l \geq x \geq 0$. For the spherical part of the shell, introducing strain-rates (15) in equation (16) we obtain:

$$\dot{e}_\theta = \theta \cot \varphi \left(1 - \cos \beta \sec \varphi + \frac{z}{R}\right) \qquad \dot{e}_\varphi = 0. \tag{18}$$

In order to have the state of stress represented by segment AB throughout the thickness, $\dot{e}_\theta$, must be positive for all values of z and φ. Thus the restriction on the geometry of the spherical part is expressed by

$$\frac{T}{D} \leq 1 - \cos \beta \sec \varphi \qquad \varphi \leq \frac{\pi}{2}. \tag{19}$$

The maximum value of $\sec \varphi$ is less than $\sec \beta$, say equal to $\sec(\beta - \psi)$, where ψ is a small quantity. The physical meaning of ψ is the angle subtended by hinge distribution at the faces of the shell. The magnitude of ψ may be of order of $2T/D$ [10]. Thus if

$$\frac{T}{D} \leq 1 - \frac{\cos \beta}{\cos \beta + \psi \sin \beta} \tag{20}$$

we have $M_\theta = 0$ in the region bounded by $\alpha \leq \varphi \leq \beta$, but no such restriction is apparently imposed by the two-moment limited-interaction surface.

The velocity fields (12) and (14) show that $[\mathrm{d}w/\mathrm{d}\varphi(\text{or } x)]$ is discontinuous at $x = l$, $x = 0$ (or $\varphi = \alpha$) and $\varphi = \beta$. This discontinuity will impose a hinge circle in these locations [9]. In such locations the $[\mathrm{d}w/\mathrm{d}\varphi \text{ (or } x)]$ vary rapidly, then $[\mathrm{d}^2w/\mathrm{d}^2\varphi \text{ (or } x)]$ must be numerically large compared to all lower derivatives, hence the strain rate vector may have the $\dot{\chi}_{(\varphi \text{ or } x)}$ component only. This discontinuity will impose a condition on the location of stress field. It could be easily shown that if the stress profile remains on the segment AB of Fig. 2, the condition on the stress field is satisfied when $M_{(\varphi \text{ or } x)}/M_0$ is maximum, i.e. in the location of hinge circles.

If the shell is to be rigid in the regions $x > l$, and $\varphi > \beta$, then a stress field can easily be constructed to satisfy all the requirements of equilibrium, continuity, and stress boundary conditions. This stress field however, will not be unique, and strain-rates are zero at these regions.

Thus, it is seen that a velocity field is found which is compatible with the stress field through the flow rule, hence the lower bound equation (8) is a complete solution.

Upper bound

An upper bound to the limit pressure can be computed by employing the kinematic approach. The expressions corresponding to the rate of energy dissipation per unit area of

the middle surface will indicate that as long as $|\dot{\chi}_\theta(T/2)| \leq |\dot{\varepsilon}_\theta|$ (i.e. the condition expressed by equation (19)), the contribution of curvature rate $\dot{\chi}_\theta$ is zero. Thus the procedure and formulation would be identical to that of Ref. [3], but with different values substituted for meridional moments M_c, M_k, and M_s. However, the upper bound formulated in Ref. [3] was in fact an exact solution within the restraints of equation (19) and hexagonal yield surface.

3. NUMERICAL RESULTS AND DISCUSSION

For the sake of direct comparison, the non-dimensional limit pressure calculated for the uniform Tresca yield surface and various approximations are tabulated in Table 1. P_T is

TABLE 1. LIMIT PRESSURE CALCULATED BY VARIOUS YIELD SURFACES

$\frac{D}{d}$	$\frac{t}{T}$	$\frac{T}{D}$	$n = \frac{t}{T}\cdot\frac{D}{d}$	$\frac{P_T}{4\sigma_0 T/D}$ (1)	$\frac{P_S}{P_T}$ (2)	$1{\cdot}25\frac{P_S}{P_T}$ (3)	$\frac{P_L}{P_T}$ (4)	$0{\cdot}618\frac{P_L}{P_T}$ (5)	$\frac{P_C}{P_T}$ (6)	Lower bound ref. [3] $\frac{P_{low}}{P_T}$ (7)
4·08*	0·50	0·006	2·09	0·268	0·91	1·14	1·40	0·87	1·04	1·33
8·38*	0·25	0·006	2·09	0·422	0·92	1·15	1·33	0·82	1·02	1·19
16·91*	0·12	0·006	2·04	0·677	0·94	1·18	1·20	0·74	1·01	1·06
4·00	0·50	0·01	2·00	0·330	0·91	1·14	1·37	0·85	1·04	1·29
8·00	0·25	0·01	2·00	0·498	0·93	1·16	1·30	0·80	1·02	1·15
16·00	0·12	0·01	2·00	0·752	0·95	1·19	1·15	0·71	1·01	1·03
4·00	0·50	0·02	2·00	0·437	0·92	1·14	1·32	0·82	1·04	1·24
8·00	0·25	0·02	2·00	0·633	0·94	1·17	1·22	0·76	1·02	1·09
16·00	0·12	0·02	2·00	0·857	0·97	1·21	1·08	0·67	1·01	1·01
4·00	0·75	0·01	3·00	0·383	0·91	1·14	1·39	0·86	1·07	1·34
8·00	0·37	0·01	3·00	0·519	0·93	1·16	1·30	0·80	1·03	1·17
16·00	0·19	0·01	3·00	0·758	0·95	1·19	1·15	0·71	1·01	1·04
4·00	0·75	0·015	3·00	0·451	0·91	1·14	1·35	0·84	1·06	1·30
8·00	0·37	0·015	3·00	0·599	0·93	1·16	1·25	0·77	1·03	1·14
16·00	0·19	0·015	3·00	0·824	0·96	1·20	1·10	0·68	1·01	1·02
4·00	0·75	0·03	3·00	0·579	0·92	1·15	1·28	0·79	1·05	1·23
8·00	0·37	0·03	3·00	0·734	0·94	1·18	1·17	0·72	1·02	1·08
16·00	0·19	0·03	3·00	0·904	0·98	1·22	1·05	0·65	1·01	1·00
4·00	1·00	0·02	4·00	0·576	0·92	1·15	1·31	0·81	1·07	1·29
8·00	0·50	0·02	4·00	0·684	0·94	1·17	1·21	0·75	1·03	1·13
16·00	0·25	0·02	4·00	0·869	0·97	1·21	1·08	0·66	1·01	1·01

* Dimensionless parameters of experimental models of Ref. [11].

non-dimensionalized by dividing by $4\sigma_0 T/D$. Other limit pressures have been normalized by dividing by P_T. Figure 6 shows plane section of the uniform Tresca yield surface (equation 9), the limited interaction (equation 11), the Sandwich approximation, and a proposed new circumscribed surface. Let the yield condition for Tresca uniform shell be denoted by f_T, that for Tresca Sandwich shell by f_S, and that for two-moment limited-interaction by f_L, then the relations between them would be [9]:

$$f_S \leq f_T \leq 1{\cdot}25\, f_S$$

$$0{\cdot}618 f_L \leq f_T \leq f_L$$

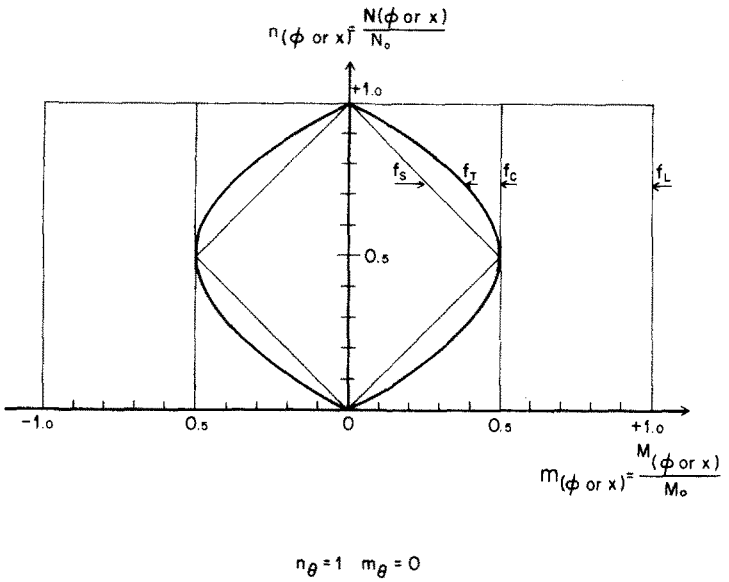

FIG. 6. The plane face of various yield surface obtained by intersection of hyper-planes $n_\theta = 1$, and $m_\theta = 0$.

According to bounding surface lemma, the same relationship must exist among the limit pressures calculated on the basis of these yield conditions. Table 1, shows that this holds true. The results indicate that the Sandwich approximation gives values of not more than 9 per cent lower than the uniform Tresca yield surface with mean deviation of -7 per cent. As the diameter ratio D/d or the thickness to diameter ratio T/D increases, the difference decreases. For the limited interaction, the difference ranges from 40 per cent to 5 per cent with mean deviation of, $+24$ per cent. Here too, the same trend with regards to D/d and T/D is observed. In comparing columns 1 and 6, one notes that the difference between the limit pressures calculated on the basis of the proposed circumscribed surface f_C and the uniform Tresca is less than 7 per cent with mean deviation, $+3$ per cent. Table 1, also includes in column 7 the values obtained from lower bound analysis of Ref. [3]. The upper bound values are identical to those of column 4.

It seems clear from comparing columns 1, 2, 4 and 6, that a complete solution for one of the yield surfaces is either a lower or upper bound for the others. It is also noted from comparing columns 2 and 3, or columns 4 and 5, that a lower bound calculated on the basis of an inscribed surface, and an upper bound on a circumscribed yield surface will differ considerably. Figure 7 shows the effect of yield surfaces on the variation of limit pressure for typical T/D and n ratios.

In the foregoing discussion it was implicitly assumed that uniform Tresca yield surface represents the actual behavior of the material better than the other surfaces. To substantiate this, experimental evidence is presented here. The first three rows in Table 1, marked with asterisks, are dimensionless parameters of the models C_3, C_2, and C_1, tested by Cloud [11]. These models are particularly chosen, since they have very little reinforcement at the junction and thus are close to the theoretical configuration, Fig. 1.

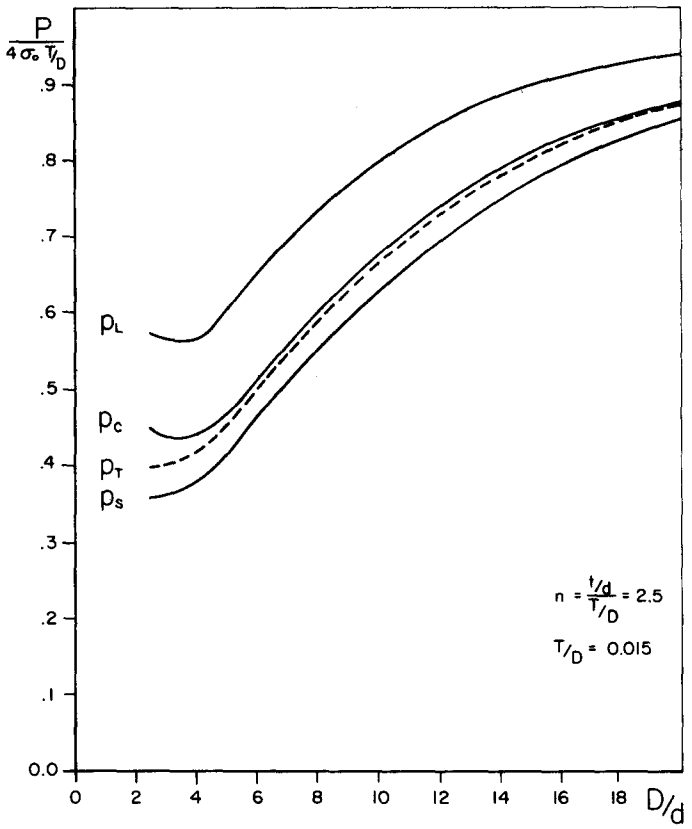

FIG. 7. The plot of limit pressure versus diameter ratio for a typical geometric configuration, calculated on the bases of Limited-interaction, uniform Tresca, Sandwich, and a newly proposed, yield surfaces.

Figure 8 shows the plots of pressure vs. circumferential strain around the junction. The experimental "limit pressures" obtained by 0·2 per cent offset strain, are indicated by V-shaped marks over the curves. The theoretical predictions based on uniform Tresca yield condition, are transformed on experimental curves and are indicated by diamond-shaped marks. The abscissa in this case has no significance. One would notice that the theoretical marks are as well placed as the experimental ones. The yield stress is assumed to be that of spherical shell. For model C_3, the difference in the yield strength of the cylindrical and spherical shell is about 50 per cent, whereas for the other models, it is less than 20 per cent. In the theoretical treatment, for the sake of simplicity, it was assumed that both shells have the same yield stress. However, if one takes the yield strength for the model C_3, to be the average of the yield strengths of the cylindrical and spherical parts, there will be much better agreement. The limit pressure, calculated on the basis of the limited interaction surface, will over-estimate considerably the strength of these vessels (see Table 1 column 4).

4. CONCLUSIONS

A complete solution, in the context of limit analysis, has been obtained for a cylinder-sphere intersecting shell. It has been shown that the limited-interaction yield surface (which

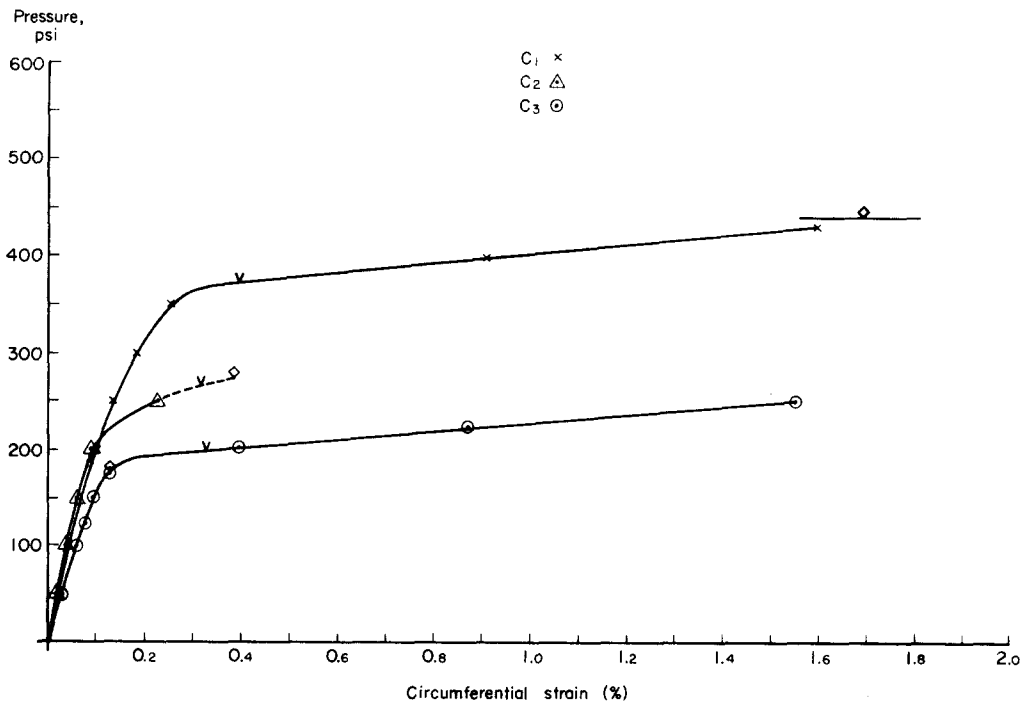

FIG. 8. Plots of test data for circumferential strain around the junction vs. pressure (Ref. [11]). V-shaped mark indicates experimental pressure and ◇—the theoretical value based on uniform Tresca.

neglects the interaction between the moments and membrane forces) is not a good approximation for the intersecting shells with small D/d and/or T/D ratios. The numerical results indicate that satisfactory results can be obtained by simply linearizing that portion of yield surface where the stress profile lies (the part of yield surface which coincides with stress point domain is often obtained by physical arguments or by making use of known solutions to similar problems). In other words, instead of attempting an over-all linearization of the exact yield surface, one must choose from the existing approximate surfaces (or any other newly proposed surface) the one which better approximates the portion of yield surface where stress profile lies. For instance, for the problem posed in this paper, the Sandwich approximation (f_S), or the partial circumscribed surface (f_C) is a much better choice than the limited-interaction (f_L). If the procedure outlined here regarding linearization is adopted, not only would one obtain accurate results, but it would also result in considerable mathematical simplification and time saving in numerical computations in contrast to the nonlinear surfaces.

Acknowledgement—The work described here, forms part of a general investigation on the openings in pressure vessels. The research is sponsored by the National Research Council of Canada (Grant A-3803) and the Subcommittee of Reinforced Openings and External Loadings of the Pressure Vessel Research Committee, Welding Research Council.

REFERENCES

[1] N. C. LIND, Plastic analysis of radial outlets from spherical pressure vessels. *J. Engng. Ind.* **86**, 193 (1964).
[2] S. S. GILL, The limit pressure for a flush cylindrical nozzle in a spherical pressure vessel. *Int. J. mech. Sci.* **6**, 105 (1964).

[3] F. ELLYIN and A. N. SHERBOURNE, The collapse of cylinder/sphere intersecting pressure vessels. *Nucl. Struc. Engng* **2**, 169 (1965) Errata, **8**, 186 (1968).
[4] F. ELLYIN and A. N. SHERBOURNE, Limit analysis of axisymmetric intersecting shells of revolution. *Nucl. Struc. Engng* **2**, 86 (1965).
[5] F. ELLYIN, Discussion of the paper, Assessment of the plastic strength of pressure vessel nozzles. *J. Engng Ind.* in press.
[6] D. C. DRUCKER and R. T. SHIELD, Limit analysis of symmetrically loaded thin shells of revolution. *J. appl. Mech.* **81**, 61 (1959).
[7] E. C. RODABAUGH *et al.*, Evaluation of experimental and theoretical data on radial nozzles in pressure vessels. USAEC. TID-24342 (1968).
[8] K. S. DINNO and S. S. GILL, Limit pressure for a protruding cylindrical nozzle in a spherical pressure vessel. *J. mech. Engng Sci.* **7**, 259 (1960).
[9] P. G. HODGE, Jr., Yield conditions for rotationally symmetric shells under axisymmetric loading. *J. appl. Mech.* **27**, 323 (1960).
[10] L. S. BEEDLE, *Plastic Design of Steel Frames*. Wiley (1958).
[11] R. L. CLOUD, The limit pressure of radial nozzles in spherical shells. *Nucl. Struc. Engng* **1**, 403 (1965).

(*Received* 10 *June* 1968; *revised* 25 *November* 1968)

Абстракт—Приводится полное решение для жестко–пластического цилиндра или сферы, пересекцючцх оболочку, подверженных внутреннему давлению. Решение представлено в виде, дающим возможность сравнить граничное давление, иодсчитанное на основе постоянной поверхности текучести Треска (эта поверхность нелинейная) с другими, линеаризованными поверхностями. Оказывается, что прямоугольное условие текучести, обычно используемое, не является пригодным приближением для малых отношений диаметров D/d, или для тонких оболочек, где T/D малое. Даются также некоторые экспериментальные доказательства для подтверждения указанных выводов.